

Electronic Supplementary Information
A Surface with Stress, Extensional Elasticity, and Bending Stiffness

Nicole Lapinski¹, Zezhou Liu³, Shu Yang⁴, Chung-Yuen Hui³, Anand Jagota^{1,2}

¹Department of Chemical and Biomolecular Engineering and ²Department of Bioengineering
Lehigh University, Bethlehem PA 18017

³Department of Mechanical & Aerospace Engineering, Cornell University, Ithaca, New York

⁴Department of Materials Science and Engineering, University of Pennsylvania, 3231 Walnut
Street, Philadelphia, PA 19104

1. Derivation of nonlinear constitutive equations of the surface

Following Milner et al.,¹ the constitutive behavior of the surface is described through a surface free energy density of the form

$$A = \sigma_0 (J_s - 1) + \frac{B}{2} (J_s - 1)^2 + \frac{k_b}{2} (\kappa - \kappa_o)^2 \quad (\text{S1})$$

The Cauchy stress tensor $\boldsymbol{\sigma}_s$ and the bending moment tensor \mathbf{m}_s in the current configuration are obtained from the free surface energy density by²⁻⁴

$$\boldsymbol{\sigma}_s = \frac{1}{J_s} \frac{\partial A}{\partial \mathbf{F}_s} \mathbf{F}_s^T = \frac{\partial A}{\partial J_s} \mathbf{1}_s = [\sigma_0 + B(J_s - 1)] \mathbf{1}_s \quad (\text{S2a})$$

$$\mathbf{m}_s = \frac{1}{J_s} \mathbf{F}_s \frac{\partial A}{\partial \boldsymbol{\kappa}_s} \mathbf{F}_s^T = \frac{1}{J_s} \frac{\partial A}{\partial (-2\Delta H)} \mathbf{F}_s \mathbf{F}_s^T = -\frac{1}{J_s} k_b (2\Delta H) \mathbf{F}_s \mathbf{F}_s^T \quad (\text{S2b})$$

where $(2\Delta H) = \kappa - \kappa_o$, we have used the identities,

$$\frac{\partial A}{\partial \mathbf{F}_s} = \frac{\partial A}{\partial \det(\mathbf{F}_s)} \frac{\partial \det(\mathbf{F}_s)}{\partial \mathbf{F}_s} = \frac{\partial A}{\partial J_s} J_s \mathbf{F}_s^{-T} \quad (\text{S3a})$$

$$\frac{\partial A}{\partial \boldsymbol{\kappa}_s} = \frac{\partial A}{\partial \text{tr}(\boldsymbol{\kappa}_s)} \frac{\partial \text{tr}(\boldsymbol{\kappa}_s)}{\partial \boldsymbol{\kappa}_s} = \frac{\partial A}{\partial (-2\Delta H)} \mathbb{I}_s^0 \quad (\text{S3b})$$

and \mathbb{I}_s^0 is the surface identity tensor in the reference configuration.

For a 2D plain strain problem, the surface stretch ratio in the out-of-plane direction is exactly one (no stretch), so there is only one *non-trivial* stretch ratio, λ_s , which is equal to J_s . Thus, we take the surface deformation gradient tensor as $\mathbf{F}_s = \lambda_s \mathbf{s} \otimes \mathbf{S}$, where \mathbf{s} and \mathbf{S} are unit tangent vectors in the current and reference configurations respectively. Using $\mathbf{1}_s = \mathbf{s} \otimes \mathbf{s}$ and $\mathbf{F}_s \mathbf{F}_s^T = \lambda_s^2 \mathbf{s} \otimes \mathbf{s}$, we have the surface stress and surface bending moment acting on the curve whose binormal direction is \mathbf{s} as

$$\boldsymbol{\sigma} = \boldsymbol{\sigma}_s \cdot \mathbf{s} = [\sigma_0 + B(\lambda_s - 1)] \mathbf{s} \quad (\text{S4a})$$

$$\mathbf{m} = \mathbf{m}_s \cdot \mathbf{s} = -\lambda_s k_b (2\Delta H) \mathbf{s} \quad (\text{S4b})$$

By convention, the surface stress is along the \mathbf{s} direction while the direction of the bending moment is out of plane.

2. FEM: Surface Element Implementation

We implemented a new 3-node surface element for the 2D plane strain simulations, which carries strain-dependent surface stresses and surface bending moments, i.e., this new surface finite element allows the surface stress to vary with stretch and surface bending moment to vary with curvature change.

In our approach, the surface elements are attached to linear C^0 continuum elements. At each node, these continuum elements have only two degrees of freedom, displacement in x- and y-axis directions, without the rotation degree of freedom. To be consistent with the shape (See Fig. S1) and to avoid violating the integrability conditions,⁵ in our case we can only ask for C^0 continuity of the surface element rather than the usual C^1 continuity using Hermitian shape functions for elements with bending. To capture the curvature change $2\Delta H$ at each node, surface elements are

applied in the following fashion: one surface element covers outer edges of two continuum elements, and two adjacent surface elements overlap over one continuum element. This way, we retain curvature change information at all points (Fig. S2). Accordingly, each surface element uses only one half of σ_0 , B and k_b as its materials properties.

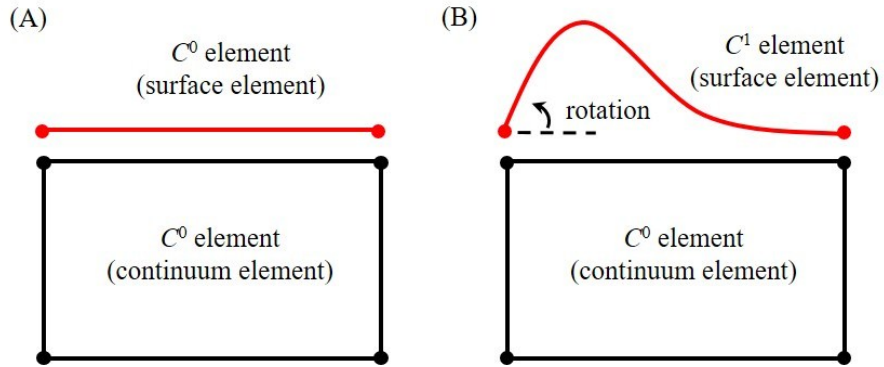


Fig. S1. Compatibility of the surface element and continuum element. (A) If the surface and continuum elements are both of C^0 continuity, they are compatible with each other; (B) if the surface and continuum elements are of C^1 and C^0 continuity respectively, incompatibility would occur between the two.

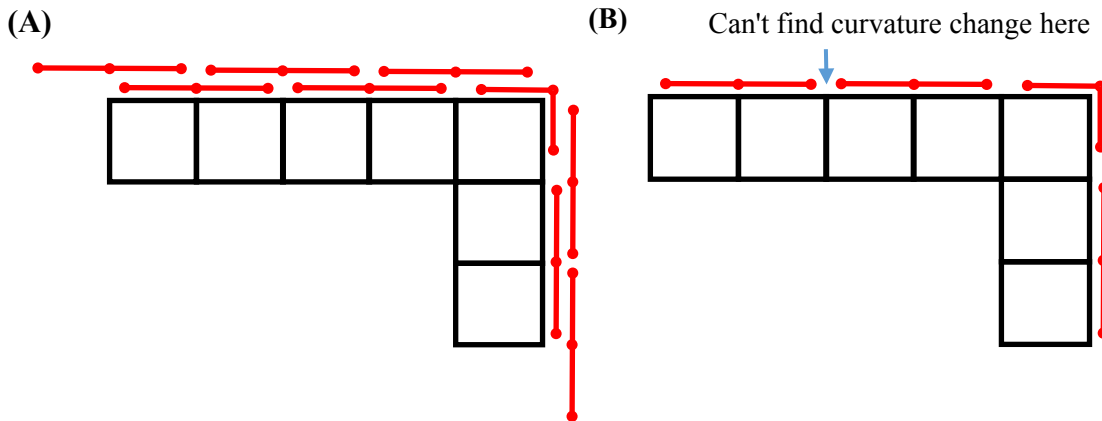


Fig. S2. Choice of pattern to apply the surface elements. Black blocks and red lines represent continuum and surface elements, respectively (A) Overlapping surface elements can represent surface stretches and surface curvature; (B) A single layer of surface elements is unable to represent curvature everywhere.

To find the change of curvature $2\Delta H$, we utilize the ideas of isoparametric finite elements. For any arbitrary 3-node surface element with nodal points (x_1, y_1) , (x_2, y_2) and (x_3, y_3) which correspond to the coordinates -1, 1 and 0 in the master element (Fig. S3), we can interpolate any point (x, y) on the surface by

$$x = \sum_{i=1}^3 N_i x_i = x(\xi) \text{ and } y = \sum_{i=1}^3 N_i y_i = y(\xi) \quad (\text{S5a, b})$$

where the N_i 's are standard shape functions: $N_1 = \frac{1}{2}\xi(\xi-1)$, $N_2 = \frac{1}{2}\xi(\xi+1)$ and $N_3 = 1-\xi^2$.

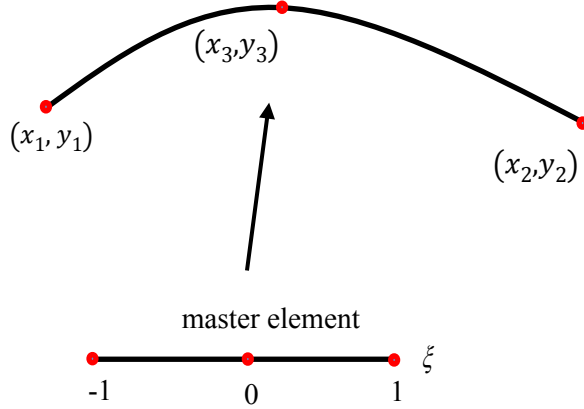


Fig. S3. Mapping from the master element to the surface element.

For a plane curve, the curvature can be calculated as

$$2H = \frac{x'y'' - y'x''}{(x'^2 + y'^2)^{3/2}} \quad (\text{S6})$$

where primes refer to derivatives with respect to ξ . Then we compute the curvature at $\xi = 0$

$$2H|_{\xi=0} = \frac{4[(y_1 + y_2 - 2y_3)(x_2 - x_1) - (x_1 + x_2 - 2x_3)(y_2 - y_1)]^2}{[(x_2 - x_1)^2 + (y_2 - y_1)^2]^{3/2}} \quad (\text{S7})$$

and take this value as the curvature of this surface element. Therefore, we can compute $2\Delta H$ by subtracting $2H|_{\xi=0}$ in the current and reference configurations, respectively.

The value of J_s , by its physical meaning, can be obtained from the ratio of the length before and after deformation. The length of the surface element is

$$l = \sqrt{(x_3 - x_1)^2 + (y_3 - y_1)^2} + \sqrt{(x_3 - x_2)^2 + (y_3 - y_2)^2} \quad (\text{S8})$$

Hence, we compute J_s by taking the ratio of the surface element length in the current and reference configurations.

The potential energy of a deformed element is

$$\Pi = -AL = -\left[A_0 + \sigma_0(J_s - 1) + \frac{B}{2}(J_s - 1)^2 + \frac{k_b}{2}(2\Delta H)^2\right]L \quad (\text{S9})$$

where L is the length of the surface element in the reference configuration.

The nodal forces are given by

$$f_i = \frac{\partial \Pi}{\partial a_i} \quad (\text{S10})$$

where a_i is the i^{th} component of the displacement vector $[x_1, y_1, x_2, y_2, x_3, y_3]^T$ in the current configuration.

The stiffness matrix of this element is given by

$$K_{ij} = -\frac{\partial f_i}{\partial a_j} \quad (\text{S11})$$

3. Thickness of Oxidized Layer by Diffusion Model

We assume that the growth of the oxidized layer is controlled by the diffusion of gaseous reactive species into PDMS, and the reaction front corresponds to the position where concentration exceeds some critical values, c_c . Since the layer thickness is much smaller than typical pattern dimensions, the region near the edge can be represented as an infinite wedge with internal angle θ_0 ($0 < \theta_0 < 2\pi$). The geometry is shown in Fig. S4.

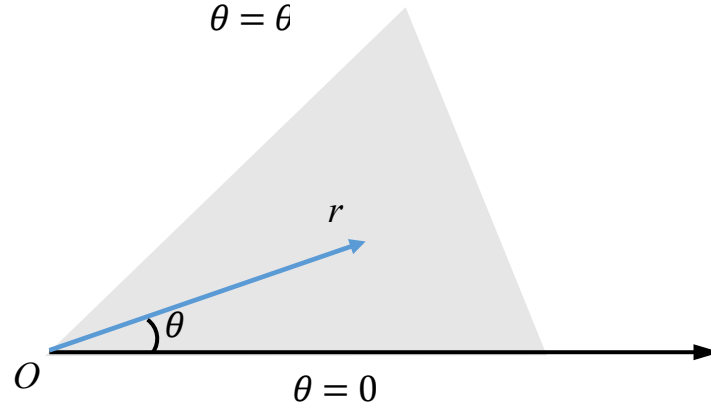


Fig. S4. Geometry of an infinite wedge in polar coordinates. The shaded region represents the wedge with the Dirichlet boundary conditions.

The tip of the wedge coincides with the origin of a polar coordinate system (r, θ) . We assume that the reaction starts at time $t = 0$. Since the surface is exposed to a constant concentration of ozone, the boundary conditions are

$$c(r, \theta = 0, t > 0) = c_0 \quad (\text{S12a})$$

$$c(r, \theta = \theta_0, t > 0) = c_0 \quad (\text{S12b})$$

Since deposition starts at $t = 0$, the initial condition is

$$c(r, 0 < \theta < \theta_0, t > 0) = 0 \quad (\text{S13})$$

In polar coordinates, the diffusion equation is

$$\partial_t c = D \left[\frac{1}{r} \frac{\partial}{\partial r} \left(r \frac{\partial c}{\partial r} \right) + \frac{1}{r^2} \frac{\partial^2 c}{\partial \theta^2} \right] \quad (\text{S14})$$

where D is the diffusion coefficient. The exact solution of (S14) subjected to the initial and boundary conditions (S13) and (S12a,b) was given by Jaeger.⁶ The solution is:

$$c(r, \theta, t) / c_0 = 1 - \frac{4}{\theta_0} \sum_{k=0}^{\infty} \sin(\nu_k \theta) \int_0^{\infty} \frac{e^{-D r w^2 / r^2}}{w} J_{\nu_k}(w) dw \quad 0 \leq \theta \leq \theta_0 \quad (\text{S15})$$

where J_{ν_k} is the Bessel function of the first kind with order $\nu_k = (2k+1)\pi / \theta_0$. Equation (S15) allows us to determine the layer thickness as a function of time and position. Since Jaeger stated the result without derivation, we will provide the detailed derivation elsewhere.

4. Representing the Oxidized Layer by Surface Properties

Fig. S5 schematically shows putative distributions of residual stress $\tau(y)$ and elastic modulus $E(y)$ along some cross sections of the oxidized layer after UVO treatment. Untreated PDMS has zero residual stress τ_{∞} and elastic modulus E_{∞} , and we assume $E_{\infty} = E(y)$. The partially oxidized PDMS has graded properties with a characteristic depth that grows due to diffusion. We replace the graded region with a layer of thickness $h(s)$ and uniform properties. We also assume that the neutral axis lies in the middle plane of the oxidized layer. Replacing the oxidized layer by a beam of thickness h , the parameters σ_0 , B and k_b of the surface can be related to the residual stress, axial stiffness and bending stiffness of the oxidized layer as

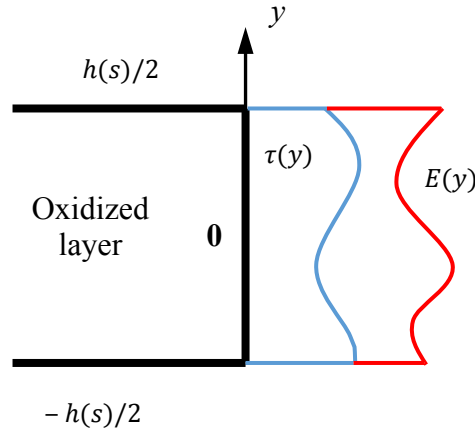


Fig. S5. Distributions of residual stress (blue curved line) and elastic modulus (red curved line) along one cross-section of the oxidized layer. The black lines bound the oxidized layer.

$$\sigma(s) = \int_{-h(s)/2}^{h(s)/2} [\tau(y) - \tau_{\infty}] dy \approx \tau_o h(s) \quad (\text{S16a})$$

$$B(s) = \int_{-h(s)/2}^{h(s)/2} [E(y) - E_{\infty}] dy \approx E_o h(s) \quad (\text{S16b})$$

$$k_b(s) = \int_{-h(s)/2}^{h(s)/2} [E(y) - E_{\infty}] y^2 dy \approx E_o \frac{h(s)^3}{12} \quad (\text{S16c})$$

where τ_o and E_o are bulk residual stress and bulk elastic modulus of the oxidized layer, and these are assumed to be independent of position.

Assume that the growth of oxidized layer on the upper edge follows the diffusion equation for an infinite wedge, and the characteristic normalized concentration of $c_c = 0.98$ identifies the boundary (reaction front) between the oxidized layer and PDMS. Thus, if the thickness $h(0)$ at

point O is known, we can solve for Dt by (S15). Furthermore, we determine the entire region of the oxidized layer once we obtain Dt . To get $h(s)$, as shown in Fig. S6 through a point P on the inner boundary we draw a line along the normal direction which intersects the upper edge at point Q . Computing the length of PQ we get $h(s)$ at point Q ; in the same fashion we determine $h(s)$ on the entire upper edge. For the vertical edge, assume that the thickness reduces linearly from $h(L)$ at the upper corner to $h(0)$ at the bottom corner; for the lower edge, assume the thickness is equal to $h(0)$ uniformly.

Therefore, if any two of $\{E_o, h(0), B(0), k_g(0)\}$ are known, by (S16b, c) we get all these four terms; once we have $h(0)$, by the above argument we can determine the thickness distribution $h(s)$ for the entire surface. Meanwhile if we know $\sigma_0(0)$ too, we can have all the surface properties by

$$\begin{aligned}\sigma_0(s) &= \sigma_0(0) \frac{h(s)}{h(0)} \\ B(s) &= E_0 h(s) = B(0) \frac{h(s)}{h(0)} \\ k_g(s) &= E_0 \frac{[h(s)]^3}{12} = k_g(0) \left[\frac{h(s)}{h(0)} \right]^3\end{aligned}\tag{S17a, b, c}$$

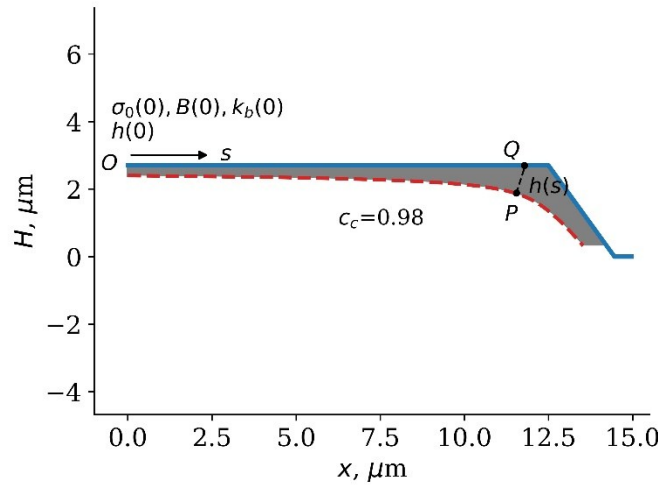


Fig. S6. Schematic drawing of oxidized layer: Strategy to represent the oxidized layer by surface properties. Through a typical point P on the reaction front where the characteristic concentration is 0.98 (red dashed line), we draw a line in the outward normal direction which intersects the surface (blue line) at point Q . The distance PQ then determines the thickness assigned to point Q . The region shaded gray represents the oxidized layer, while the blank region below the red dashed line represents the unreacted PDMS. The thickness of the oxidized layer is used to compute (spatially varying) surface stress, surface extensional elasticity, and surface bending elasticity.

5. Parameter Estimation for UV Ozone Treated PDMS

To get a reasonable starting point for the fitting procedure of UV Ozone treated PDMS samples, we first extract an approximate surface stress value for each data point. We use the same fitting procedure as described in Section 2.5 of the main text to obtain an initial approximate value for the surface stress for a given applied stretch. Specifically, we use Fig. 3B to determine the elastocapillary number σ_0/Ew for a given applied in-plane stretch and measured normalized amplitude. Since the Young's modulus of the PDMS and wavelength are known independently by direct measurements, we can so calculate the surface stress value for each data point. Next, we use a least-squares fitting to find the relationship between the surface stress so estimated and the applied stretch. As an example, the results in Fig. S7 give us estimates of $\sigma_0(0) \approx 2.0 \text{ N/m}$ and $B(0) \approx 20 \text{ N/m}$.

The small offset between stretch/loading and release/unloading seen in Figure S7 is also observed in Figures 5B,C but not in Figure 4. This effect is small in that stress-stretch is nearly reversible. Also, results were reproducible over several cycles, and from these two observations we conclude that the surface behaves elastically in the main. However, the results do indicate some surface inelasticity, which would be interesting to examine in a follow-up study.

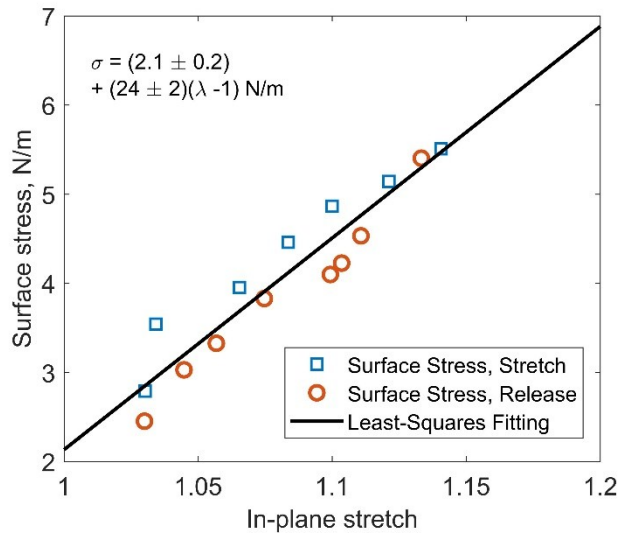


Fig. S7. Estimation of surface stress and extensional elasticity. The blue squares and red circles represent the extracted surface stresses during the stretch and release process respectively, and the solid line represents the least-square fit.

6. Thickness Adjustment for FEA

Adjusting the thickness of the oxidized layer preferentially affects the profiles at the corners while only marginally affecting the deformation elsewhere. In Fig. S8, we fit the height reduction versus stretch with various thicknesses. It shows that if we maintain the product of the oxidized layer's thickness and its bulk elastic modulus, we would still get as good a fit to the height reduction versus stretch (Fig. S8A), but might not get the characteristic sharp edge shape at the

corners (Fig. S8B). In particular, the results indicate that when the thickness is less than ~ 100 nm, FEM can not capture the corner feature; on the other hand, when the thickness is bigger than ~ 300 nm, we reproduce the feature by our FE model, and further increasing the thickness doesn't change the profiles much. Since experimentally, it is known that the oxidized region has thickness of about a few hundred nm, we choose $h(0) \approx 0.3 \mu\text{m}$, at the lower end of the range that works for fitting the 50-micron PDMS sample.

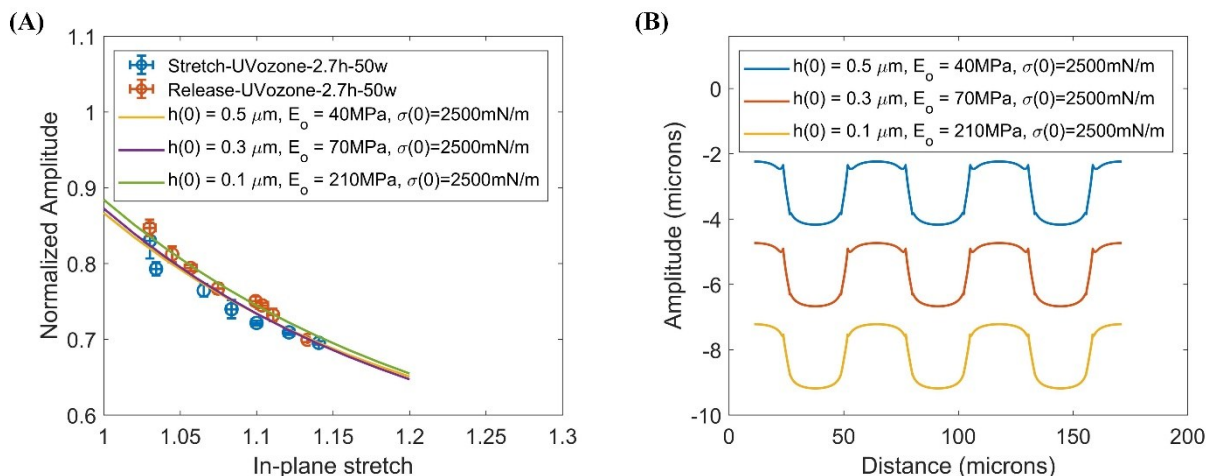


Fig. S8. Results of varying the oxidized layer thickness and bulk modulus for a stretching experiment for patterned PDMS samples exposed to UVO for 60 minutes with amplitude $a = 1.35 \mu\text{m}$ and wavelength $w = 50 \mu\text{m}$. (A) Normalized height versus in-plane stretch for 50-micron PDMS sample. The yellow, purple and green lines represent the thickness $h(0)$ of 0.5, 0.3 and 0.1 microns respectively. (B) Line scans for the thickness $h(0)$ of 0.5, 0.3 and 0.1 microns cases respectively.

7. Line Scan Fitting for 40-Micron and 30-Micron Samples

The linescan fits for 40-micron and 30-micron samples are shown in Fig. S9 with the fitting parameters provided in Table 1 of the main text. Notice that in Fig. S9 an overshoot of the line scans occurs locally near the edges of each ridge. For nearly flat regions, this method provides accurate height measurements ($\pm 3 \text{nm}$). However, interferometric measurements fail when the surface has significant slope (typically > 25 degrees). For any typical ridge, the data are therefore reliable as one approaches either the left or right edges from the middle of the ridge. However, data on the left side of the left edge or right side of the right edge are not reliable. Therefore, we can reliably conclude that the edges of each ridge have ear-like “overshoots” but it is difficult to trust their magnitude from these experimental measurements. We should point out that this effect is local. Away from these sharp edges, the line scans are quite accurate and match the FE result very well.

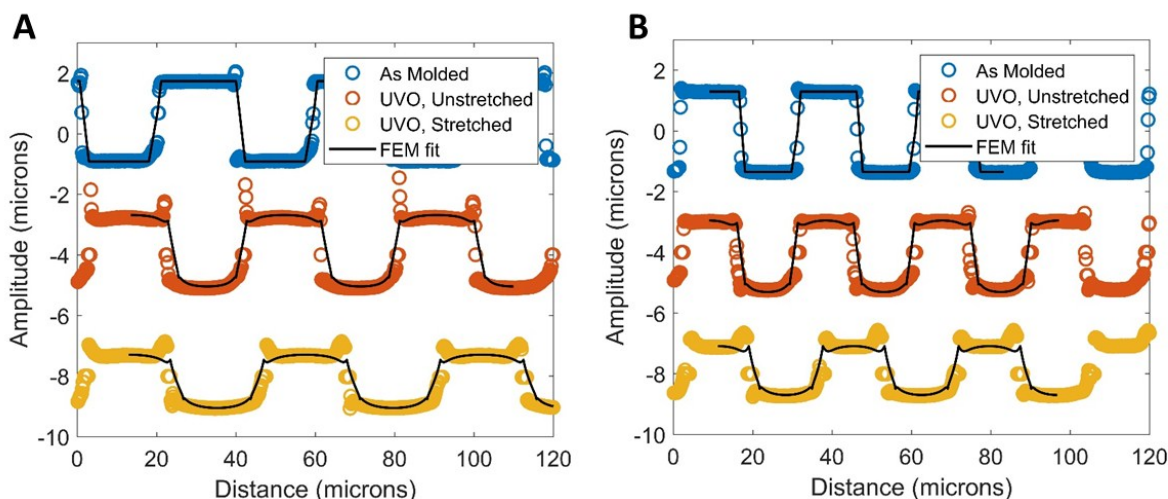


Fig. S9. Line scans for $a = 1.35 \mu\text{m}$ and $w = 40 \mu\text{m}$ and $30 \mu\text{m}$ UVO PDMS are shown before UVO exposure and after UVO exposure (unstretched and maximum stretched states). FEM fits are also shown. (A) $40 \mu\text{m}$ (B) $30 \mu\text{m}$

8. Effect of Soft Layer on Stiff PDMS on Amplitude Reduction

For one of the untreated PDMS negative control samples, we observed consistent disagreement, between our FEM predictions and experimental results for the normalized amplitude versus stretch (Fig. S10). Overall, this is an exception to the majority of cases analyzed where FEM results matched amplitude reduction with stretch. However, we could bring the simulation and experiment into better agreement if we assumed the top 5 microns layer to be softer than the bulk, say by reducing its Young's Modulus

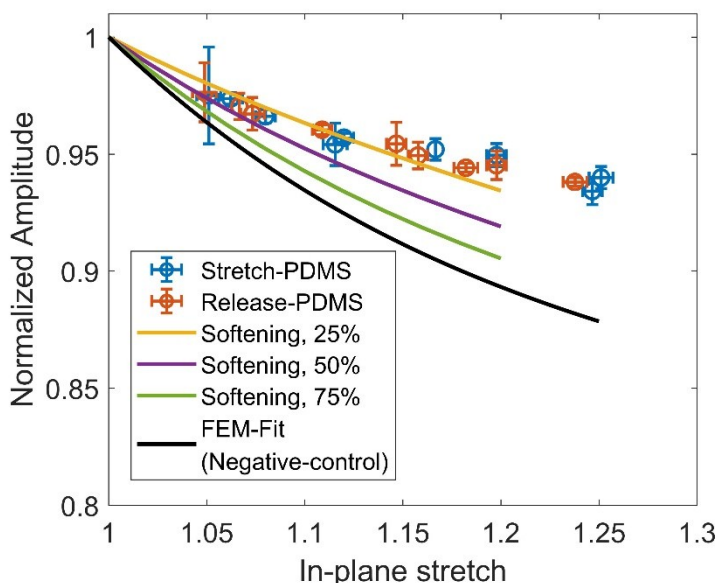


Fig. S10. Normalized amplitude versus stretch for an untreated PDMS samples with $a = 1.35 \mu\text{m}$ and $w = 30 \mu\text{m}$. In this case the deformation is small but we found a consistent disagreement between the finite element prediction and experiment. Experiments for the $w=50 \mu\text{m}$ sample shown in Fig. 2B of the main manuscript are in significantly better agreement with FEM results although the small discrepancy in that case is also that FEM calculations predict a slightly greater

reduction in amplitude than measured. FEM simulation results for the gel samples and UVO-PDMS samples were all able to match experiment very well. It is known that near-surface moduli can be lower than that of the bulk. Interestingly, our calculations show that reducing the near surface modulus does in fact improve the comparison between FEM and experimental results. While the discrepancy for this sample shown in Fig. S10 is not fully resolved, in the context of the majority of the experimental data and its FEM analysis we believe this case to be an exception that does not affect our overall conclusions.

9. REFERENCES

1. Milner, S.; Joanny, J.; Pincus, P., Buckling of Langmuir monolayers. *EPL (Europhysics Letters)* **1989**, *9* (5), 495.
2. Green, A. E.; Naghdi, P. M.; Wainwright, W., A general theory of a Cosserat surface. *Archive for Rational Mechanics and Analysis* **1965**, *20* (4), 287-308.
3. Simo, J. C.; Fox, D. D.; Rifai, M. S., On a stress resultant geometrically exact shell model. Part III: Computational aspects of the nonlinear theory. *Computer Methods in Applied Mechanics and Engineering* **1990**, *79* (1), 21-70.
4. Gao, X.; Huang, Z.; Qu, J.; Fang, D., A curvature-dependent interfacial energy-based interface stress theory and its applications to nano-structured materials:(I) General theory. *Journal of the Mechanics and Physics of Solids* **2014**, *66*, 59-77.
5. Zienkiewicz, O. C.; Taylor, R. L.; Zhu, J. Z., *The Finite Element Method: Its Basis and Fundamentals (sixth edition)*. Butterworth-Heinemann: 2005.
6. Jaeger, J., LIV. Heat conduction in a wedge, or an infinite cylinder whose cross-section is a circle or a sector of a circle. *The London, Edinburgh, and Dublin Philosophical Magazine and Journal of Science* **1942**, *33* (222), 527-536.